Multiple Autophosphorylation Is Essential for the Formation of the Active and Stable Homodimer of Heme-Regulated eIF2α Kinase†

Bettina N. Bauer, Maryam Rafie-Kolpin, Linrong Lu, Anping Han, and Jane-Jane Chen*

Harvard−MIT Division of Health Sciences and Technology, Massachusetts Institute of Technology, Cambridge, Massachusetts 02139

Received May 14, 2001; Revised Manuscript Received July 23, 2001

ABSTRACT: In heme-deficient reticulocytes, protein synthesis is inhibited due to the activation of heme-regulated eIF2α kinase (HRI). Activation of HRI is accompanied by its phosphorylation. We have investigated the role of autophosphorylation in the formation of active and stable HRI. Two autophosphorylated species of recombinant HRI expressed in *Escherichia coli* were resolved by SDS−PAGE. Both species of HRI were multiply autophosphorylated on serine, threonine, and to a lesser degree also tyrosine residues. Species II HRI exhibited a much higher extent of autophosphorylation and thus migrates slower in SDS−PAGE than species I HRI. Similarly, HRI naturally present in reticulocytes also exhibited these species with different degrees of phosphorylation. Importantly, in heme-deficient intact reticulocytes, inactive species I HRI was converted completely into species II. We further separated and characterized these two species biochemically. We found that species I was inactive and had a tendency to aggregate while the more extensively autophosphorylated species II was an active heme-regulated eIF2α kinase and stable homodimer. Our results strongly suggest that autophosphorylation regulates HRI in a two-stage mechanism. In the first stage, autophosphorylation of newly synthesized HRI stabilizes species I HRI against aggregation. Although species I is an active autokinase, it is still without eIF2α kinase activity. Additional multiple autophosphorylation in the second stage is required for the formation of stable dimeric HRI (species II) with eIF2α kinase activity that is regulated by heme.

In heme deficiency, protein synthesis in reticulocytes is inhibited by phosphorylation of the α-subunit of the eukaryotic initiation factor 2 (eIF2)[1] as the result of the activation of heme-regulated eIF2α kinase (HRI; reviewed in ref *1*). This phosphorylated eIF2 binds with high affinity to eIF2B, thereby inhibiting the GTP/GDP exchanging activity of eIF2B which is required for the recycling of eIF2 in translational initiaton. Since eIF2B is limiting, phosphorylation of a fraction of eIF2α is sufficient to inactivate all available eIF2B and halt translation (*2*; reviewed in ref *3*).

HRI is expressed predominantly in immature erythroid cells, i.e., reticulocytes and bone marrow (*4*). One of its physiological roles is to regulate protein synthesis according to heme availability (reviewed in ref *1*). In the presence of heme HRI is inactive. The inactive state is maintained by intersubunit disulfide bond formation promoted by the binding of heme (*5*, *6*). Heme binds to the regulatory heme-binding site recently identified in the kinase insertion domain (*7*). In addition to heme deficiency, various other conditions such as heat shock, oxidative stress, and the presence of denatured proteins, sulfhydryl reagents, and heavy metal ions have been shown to activate HRI in reticulocyte lysates (reviewed in refs *8*−*10*). However, the mechanism of HRI activation is not yet known.

In addition to HRI, three other eukaryotic eIF2α kinases have been cloned and characterized. The double-stranded RNA-dependent protein kinase (PKR) is present in most mammalian cells at a low constitutive level (reviewed in refs *10* and *11*). The pancreatic eIF2α kinase (PEK) (*12*), identical to PERK (*13*), which resides in the endoplasmatic reticulum (ER) is found in the rat, mouse, human, *Drosophila melanogaster*, and *Caenorhabditis elegans* (*14*). GCN2 has been identified in yeast (*15*), as well as *D. melanogaster* (*16*), *Neurospora crassa* (*17*), and mammals (*18*). The highest levels of PEK and GCN2 occur in secretory tissues (*13*, *14*) and in liver and brain (*18*), respectively.

These eIF2α kinases share extensive homology within catalytic domains (*12*, *13*, *19*−*23*) and phosphorylate eIF2α on the Ser51 residue (*12*, *13*, *24*, *25*). However, regulatory domains and regulatory mechanisms among eIF2α kinases are distinct and allow them to respond to different environmental signals. PKR is activated by binding of dsRNA to the two N-terminal dsRNA-binding motifs (reviewed in ref *26*) and has been implicated in many cellular processes such as cellular signal transduction, cell growth, apoptosis, differentiation, tumor suppression, and antiviral defense (reviewed in refs *11* and *27*). PEK responds to ER stress signal and has a lumenal domain which resembles the stress-sensory

† This study was supported by National Institutes of Health Grants DK-53223 and DK-16272 to J.-J.C. M.R.-K. is a recipient of National Institutes of Health Postdoctoral Fellowship DK-09773.

* Corresponding author: E25-545, MIT, Cambridge, MA 02139. Tel: (617) 253-9674. Fax: (617) 253-3459. E-mail: j-jchen@mit.edu.

[1] Abbreviations: HRI, heme-regulated eIF2α kinase; eIF2α, α-subunit of eukaryotic initiation factor 2; Wt, wild type; K196R HRI, mutation of the Lys^{196} of mouse HRI to Arg; P-Ser, phosphoserine; P-Thr, phosphothreonine; P-Tyr, phosphotyrosine; MW, molecular weight; S, supernatant; P, pellet; AP, alkaline phosphatase; PKR, double-stranded RNA-dependent protein kinase; ER, endoplasmatic reticulum; DTT, 1,4-dithiothreitol.

10.1021/bi010983s CCC: $20.00
Published on Web 08/31/2001

domain of the ER-resident kinase, Ire1 (*13*). GCN2 is activated under amino acid and other nutrient starvation through a C-terminal domain that contains a His-tRNA synthase-like sequence (reviewed in ref *28*).

For each of these eIF2α kinases, activation is accompanied by autophosphorylation. Following dimerization, PKR undergoes intermolecular autophosphorylation (*29*, *30*) on several serine and threonine residues (*31*). Mutation of Thr258 to alanine reduces but does not abrogate PKR function, and mutation of two additional autophosphorylation sites, Ser242 and Thr255, to alanine further attenuates its kinase activity. Site-directed mutagenesis studies indicate that Thr446 and Thr451 in the activation loop are required for high-level kinase activity in vivo and in vitro (*32*, *33*). Mutational analysis also showed that GCN2 autophosphorylation occurs on Thr882 and Thr887 in the activation loop (*32*). Interestingly, both threonine residues are conserved in subdomain VIII of all eIF2α kinases (*13*, *32*). The activation of HRI is also accompanied by its phosphorylation. Uma et al. (*34*) have shown that, in heme-deficient reticulocyte lysates, newly translated recombinant HRI undergoes autophosphorylation and is transformed into active eIF2α kinase. However, the role of autophosphorylation in the regulation of HRI in intact cells remains to be determined.

In this study, we investigated the different species of HRI in intact reticulocytes in vivo with particular focus on autophosphorylation in the production of active and stable HRI. We found that multiple autophosphorylation of HRI on serine, threonine, and tyrosine residues occurs at two stages. Autophosphorylation at the first stage is required to prevent rapid aggregation of HRI. The second stage autophopshorylation of HRI is required for its eIF2α kinase activity and stabilization of HRI as a homodimer.

EXPERIMENTAL PROCEDURES

Materials. Escherichia coli BL21 cells and pET28a vector were obtained from Novagen. Isopropyl β-D-thiogalactopyranoside (IPTG) and imidazole were obtained from Sigma. The rTEV protease was from Gibco Life Technologies, and the nitrocellulose membrane was from Schleicher & Schuell. The antibodies were purchased from Pharmacia Biotech [anti-$(His)_6$ monoclonal antibody], Zymed (anti-phosphoserine polyclonal antibody, anti-phosphothreonine monoclonal antibody), Upstate Biotechnology (anti-phosphotyrosine monoclonal antibody), and Promega (horseradish peroxidase conjugated second antibody). The chemiluminescent reagent was from NEN Life Sciences. The HiTrapQ column was obtained from Amersham Pharmacia Biotech.

Subcloning of Mouse HRI cDNA into the Bacterial Expression Vector and Generation of K196R Mutant HRI. Mouse HRI cDNA was cloned from mouse erythroleukemic cells and will be published elsewhere. The full-length mouse HRI cDNA was subcloned into pET28a vector with a N-terminal $(His)_6$ tag. The K196R point mutation of mouse HRI was produced by site-directed mutagenesis as described previously (*35*) and confirmed by sequencing. Position 196 in mouse HRI corresponds to position 199 in rabbit HRI due to a three amino acid deletion in the N-terminal domain.

Expression of HRI in E. coli BL21 Cells. Wild-type (Wt) and mutant K196R HRI were expressed in *E. coli* BL21 cells. Bacterial cultures were grown at 37 or 22.5 °C to an OD_{600} of 0.6 and then induced with 100 μM IPTG for the indicated time periods. Cells from 2.5 mL cultures were harvested by centrifugation at 16000*g* for 20 s at 4 °C and lysed by sonication in 1.5 mL of lysis buffer containing 50 mM sodium phosphate buffer, pH 8.0, 300 mM NaCl, and 10 mM imidazole. Cell lysates were centrifuged at 16000*g* for 15 min at 4 °C. Pellets were resuspended in 1.5 mL of lysis buffer and were washed with 0.5 mL of lysis buffer three times. Where indicated, fractionation of soluble HRI by 100000*g* centrifugation was performed for 3 h at 4 °C.

Phosphoamino Acid Analysis. Mouse HRI was labeled with 2.5 mCi of $[^{32}P]P_i$ orthophosphate (28.3 Ci/μmol) during expression in 50 mL of culture for 8 h at 13 °C. Cells were harvested and lysed as described above. HRI was separated on a 7.5% preparative SDS−polyacrylamide gel and was transferred to a PVDF membrane. Radiolabeled HRI was excised from the PVDF membrane and hydrolyzed with 6 M HCl at 110 °C for 60 min. The liquid hydrolysate was dried by Speedvac and reconstituted in distilled H_2O. Hydrolyzed phosphoamino acids were separated by two-dimensional thin-layer electrophoresis as described (*36*).

Protein Kinase Assays and Western Blot Analysis. Protein kinase assays of HRI were performed as described previously (*5*) using purified rabbit eIF2 or recombinant yeast $(His)_6$-eIF2α (*37*) as a substrate. Cell lysates, supernatant and pellet fractions of 16000*g* or 100000*g* centrifugation, or purified HRI were separated by 10% SDS−PAGE and transferred to the nitrocellulose membrane using a mini trans-blot transfer cell at 80 V, 4 °C, for 2 h. The blots were blocked with 5% bovine serum albumin in TBST [10 mM Tris-HCl, pH 7.4, 0.9% NaCl (TBS), 0.05% Tween 20] for 30 min at room temperature and incubated for 3 h at room temperature with anti-$(His)_6$ monoclonal antibody, anti-phosphoserine polyclonal antibody, anti-phosphothreonine monoclonal antibody, or anti-phosphotyrosine monoclonal antibody. Blots to be processed with anti-mouse HRI antibody were blocked first with 5% nonfat milk in TBS containing 0.5% Tween 20 for 1 h at room temperature and then incubated with antibody for 1 h at room temperature. Anti-eIF2α(P) and anti-eIF2α antibodies were used according to refs *38* and *39*, respectively. Immunoreactive proteins were visualized with chemiluminescent reagents after incubation with horseradish peroxidase conjugated second antibody.

Purification of $(His)_6$-HRI by Ni^{2+}−Agarose Chromatography. Soluble $(His)_6$-HRI from 16000*g* supernatant was purified from a 250 mL expression (5 h at 22.5 °C) using Ni^{2+}−agarose column chromatography. Cell lysate prepared as described above was loaded onto 0.5 mL of Ni^{2+}−agarose matrix at a flow rate of 0.5 mL/min. The column was washed with 5 mL of 50 mM sodium phosphate buffer, pH 8.0, containing 300 mM NaCl and 20 mM imidazole. HRI was eluted with 500 mM imidazole in 50 mM sodium phosphate (pH 8.0) and 300 mM NaCl. Insoluble $(His)_6$-HRI from a 500 mL expression (3 h at 37 °C) was solubilized with 8 M urea. The urea denatured $(His)_6$-HRI was dialyzed stepwise against decreasing concentrations of urea (6 M, 4 M, 2 M) and finally phosphate-buffered saline (PBS) containing 10% glycerol and 10 mM 2-mercaptoethanol. Insoluble HRI was then purified using Ni^{2+}−agarose column chromatography under native conditions as described above.

CD Spectroscopy. CD spectra of purified soluble and insoluble HRI were obtained using the circular dichroism

spectrometer model 202 from Aviv Instruments, Inc. (Lakewood, NJ). Proteins (24 μM in 50 mM phosphate buffer, pH 7.8) were placed in a 0.2 cm cell length cuvette, and spectra were obtained at 4 °C by scanning from 185 to 300 nm at 6 s/nm with a bandwidth of 1.0 nm and a resolution of 0.2 nm. For the spectrum of heme-bound HRI, HRI was saturated with 100 μM heme (15 min at 30 °C). Excess free heme was removed by dialysis against 50 mM phosphate buffer, pH 7.8.

Sephacryl S-400 Column Chromatography. Sephacryl S-400 column chromatography was performed using a 1 × 50 cm column with a buffer containing 30 mM Tris, pH 7.6, 50 mM KCl, 0.1 mM EDTA, 10% glycerol, 2 mM DTT, and 0.1% Triton X-100. Fractions of 1 mL were collected. The column was calibrated with the following molecular size standards: thyroglobulin (670 kDa), ferritin (440 kDa), catalase (230 kDa), aldolase (150 kDa), and hemoglobin (64 kDa). The void (8×10^6 Da) eluted at 14 mL.

Preparation of Lysates from Mouse Reticulocytes. The generation of $HRI^{-/-}$ mice and the preparation of mouse reticulocyte lysates will be published elsewhere. In brief, blood of phenylhydrazine-treated, 14-week-old male mice containing 90% reticulocytes was washed three times with PBS supplemented with 0.09% glucose and lysed with an equal volume of ice-cold, autoclaved deionized water in ice for 15 min. Reticulocyte lysates were prepared by centrifugation at 16000*g* (4 °C) for 30 min.

HiTrapQ Chromatography of HRI in Mouse Reticulocyte Lysates. HiTrapQ chromatography was performed according to the Amersham Pharmacia Biotech protocol using a 1 mL HiTrapQ column (0.7 × 2.5 cm). Reticulocyte lysates prepared from 560 μL of blood were centrifuged at 100000*g* for 3 h at 4 °C. The supernatant was diluted 10-fold with buffer containing 20 mM Tris, pH 8.0, 0.2 M NaCl, 1 mM EDTA, 10% glycerol, and 5 mM DTT, filtered through a 0.45 μm filter, and loaded onto the column. The column was washed with 12 mL of the same buffer. Elutions were performed with 12 mL each of the buffer with 0.2, 0.3, 0.35, 0.4, and 1 M NaCl. Fractions of 0.75 mL were collected.

RESULTS

Multiple Autophosphorylation, Activity, and Solubility of HRI. Recombinant HRI was produced using the *E. coli* pET expression system. This system was used for studying the autophosphorylation of eukaryotic kinases since bacteria contain little endogenous serine/threonine or tyrosine kinase activity (reviewed in ref *40*; data not shown). Mouse HRI cDNA was subcloned into a pET vector with an N-terminal $(His)_6$ tag to facilitate the purification of recombinant HRI. After expression, cell extracts were subject to 16000*g* centrifugation in order to separate unfolded, insoluble HRI in the pellet from the folded, soluble HRI in the supernatant. Expression at 37 °C yielded recombinant HRI that was mainly insoluble and subject to significant proteolysis (not shown). Expression at 22.5 °C significantly increased the proportion of HRI in the soluble fraction (Figure 1). Expression for 8 h appeared to be optimal with respect to the yield of soluble HRI. Western blot analysis using anti-HRI antibody revealed two species of soluble HRI which were designated as species I and II according to their electrophoretic mobilities (Figure 1A). Species I is the faster migrating soluble HRI; species II was the slower migrating form. Species I was produced first followed by the appearance of species II. Insoluble HRI migrates slightly faster than soluble HRI species I.

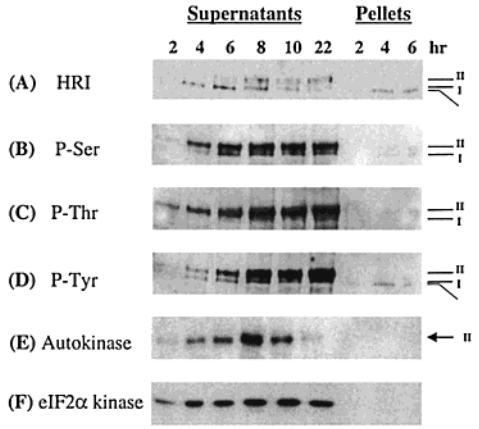

FIGURE 1: Multiple autophosphorylation of soluble HRI. HRI was expressed in *E. coli* at 22.5 °C for the indicated time periods as described in Experimental Procedures. Equal volumes of 16000*g* supernatant (S) and pellet (P) fractions were subjected to 10% SDS−PAGE. The amount of expressed HRI at each time point was determined by Western blot analysis using anti-HRI N-terminus antibody (panel A). The two soluble HRI species are designated as I and II, and the insoluble HRI in the pellet is also marked. The extent of HRI autophosphorylation was assessed using anti-phosphoserine (panel B), anti-phosphothreonine (panel C), and anti-phosphotyrosine (panel D) antibodies. Autokinase (panel E) and eIF2α kinase (panel F) activities of HRI in the supernatants and pellets were also analyzed.

Phosphorylation states of the various species of HRI were examined by Western blot analysis using antibodies raised against phosphoserine (P-Ser), phosphothreonine (P-Thr), and phosphotyrosine (P-Tyr) (Figure 1B−D). Recombinant HRI was the major phosphoprotein in *E. coli* extracts. The slower migrating species II was extensively phosphorylated on serine, threonine, and tyrosine residues. The faster migrating species I was also multiply phosphorylated on serine, threonine, and tyrosine residues but to a much lesser extent. Insoluble HRI in the pellets was barely phosphorylated. These results demonstrate that the shift in the electrophoretic mobility of HRI correlates with the extent of multiple phosphorylation of HRI. In addition, the phosphorylation of HRI appears to correspond with its solubility.

The activation of HRI has been observed to correlate with its phosphorylation (reviewed in refs *9* and *10*). This suggests that only the autophosphorylated soluble species of HRI can function as active kinase. As expected, no endogenous eIF2α kinase activity was detectable in *E. coli* before induction of expression of HRI (not shown). Neither eIF2α kinase nor autokinase activity was detected in the pellet fractions, indicating that insoluble HRI was in an inactive conformation (Figure 1E,F). In contrast, soluble HRI was an active autokinase (Figure 1E) and phosphorylated eIF2α (Figure 1F). As shown in Figure 1B−D, HRI underwent autophosphorylation in vivo during expression. HRI expressed at 10 and 22 h had undergone nearly maximal autophosphorylation and thus could only incorporate little additional γ-^{32}P during in vitro kinase assays (Figure 1E).

To test our hypothesis that multiple autophosphorylation of HRI increases its solubility, further fractionation by high-speed centrifugation at 100000*g* was performed. The aim of

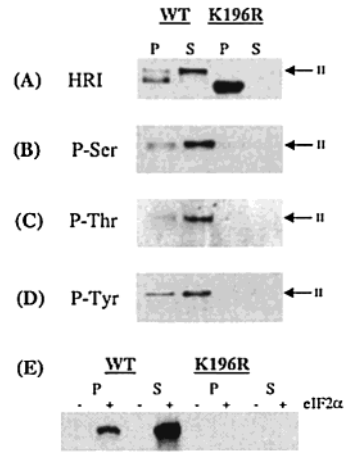

FIGURE 2: Insolubility of mutant K196R HRI. Wild-type and K196R HRI were expressed for 8 h at 22.5 °C. The 100000*g* supernatant (S) and pellet (P) fractions were prepared as described under Experimental Procedures and subjected to 10% SDS−PAGE followed by Western blot analysis using anti-HRI (panel A), anti-phosphoserine (panel B), anti-phosphothreonine (panel C), and anti-phosphotyrosine (panel D) antibodies. The eIF2α kinase activities of HRI were also analyzed (panel E).

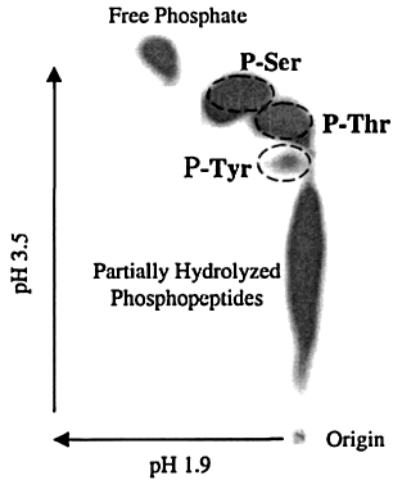

FIGURE 3: Phosphoamino acid analysis of HRI labeled in vivo. HRI was expressed in the presence of [^{32}P]inorganic phosphate in *E. coli* as described in Experimental Procedures. [^{32}P]HRI was hydrolyzed, and the hydrolyzed phosphoamino acids were separated by two-dimensional thin-layer chromatography. The position of each phosphoamino acid was determined by using 0.6 μg each of the standards and staining with ninhydrin (dotted circles). The arrows indicate the direction of migration.

this centrifugation was to separate the aggregated yet soluble HRI (species I) from the multiply autophosphorylated and active HRI (species II). As shown in Figure 2A, the 100000*g* supernatant contained exclusively species II HRI whereas the 100000*g* pellet had mainly species I HRI. Species II HRI in the 100000*g* supernatant was phosphorylated extensively on serine, threonine, and tyrosine residues whereas the faster migrating species I was poorly phosphorylated (Figure 2B−D) and its phosphorylation was detectable only following much longer exposures. HRI in the 100000*g* supernatant was a very active eIF2α kinase (Figure 2E). In contrast, HRI in the pellet fraction had only slight eIF2α kinase activity which may originate from small amounts of slower migrating species trapped in the pellet.

To ascertain whether autophosphorylation is responsible for the observed mobility shift of HRI, the K196R mutant of mouse HRI was prepared and expressed. The corresponding K199R mutation in rabbit HRI was reported earlier to have extremely poor autokinase activity (*41*). As compared to the Wt HRI, K196R HRI underwent autophosphorylation extremely poorly (Figure 2B−D) and had an even faster electrophoretic mobility than the insoluble Wt HRI in the pellet (Figure 2A). This result demonstrates that phosphorylation of HRI in *E. coli* is due to autophosphorylation. Furthermore, K196R HRI was highly insoluble; no K196R HRI was detected in the 100000*g* supernatant. These results demonstrate that autophosphorylation of HRI not only is essential to eIF2α kinase activity of HRI but also influences its solubility.

Autotyrosine Kinase Activity of HRI. HRI has the consensus sequence for the serine/threonine kinases (*42*) and phosphorylates the substrate eIF2α at the Ser51 residue (*12*, *13*, *24*, *25*). Thus, it was surprising to detect HRI phosphorylation at tyrosine residues. To confirm the presence of phosphotyrosine in HRI, mouse HRI expressed in *E. coli* was labeled with [^{32}P]inorganic phosphate in vivo and subjected to partial acid hydrolysis followed by two-dimensional thin-layer electrophoresis and chromatography. The result of phosphoamino acid analysis showed that HRI was autophosphorylated on Ser, Thr, and Tyr residues (Figure 3). However, HRI was mainly phosphorylated at Ser and Thr residues, the ratio of Tyr:Thr:Ser phosphorylation being 1:12:31. Mouse HRI contains 16 Tyr, 30 Thr, and 51 Ser residues. Thus, the degree of autophosphorylation of HRI at tyrosine is much less than that at serine and threonine, and the strong signal seen in Figure 1D is due to the higher sensitivity of P-Tyr antibody. Autotyrosine kinase activity of HRI was also observed in immunoaffinity-purified Wt HRI from rabbit reticulocytes and recombinant Wt HRI (but not the K199R mutant) expressed in insect cells (data not shown). Similarly, as shown in Figure 2, inactive K196R mouse HRI did not undergo tyrosine phosphorylation. Thus, tyrosine phosphorylation of HRI is an intrinsic property of HRI, but its functional significance remains to be investigated.

Molecular Sizes of the Soluble HRI Species. To understand the basis for the biochemical difference between HRI species I and II, the molecular sizes of the HRI in the 16000*g* supernatant and 100000*g* fractions were subjected to S-400 gel filtration study (Figure 4A−D). The two HRI species present in the 16000*g* supernatant eluted differently upon gel filtration (Figure 4A). Species I, which was present in the pellet of 100000*g*, was found in the void with an apparent MW of about 8×10^6 Da or larger (Figure 4C). High-salt washes with 0.5 M KCl did not release species I from the pellet. Therefore, this species I HRI is not associated with cellular organelles such as ribosomes or membranes. Species I HRI is most likely the aggregated oligomer of HRI.

HRI species II, which was present in the 100000*g* supernatant, eluted with an apparent MW of 640 kDa (Figure 4B). After removal of the His tag, species II HRI eluted similarly to HRI from mouse reticulocyte lysates with an apparent MW of 420 kDa (Figure 4D) due to its elongated shape (*41*). It is well established by works of ours and others that HRI in reticulocytes is present as a dimer (*6*, *43*, *44*). This is demonstrated by gradient centrifugation and chemical cross-linkings (*6*). Since the presence of the His tag did not

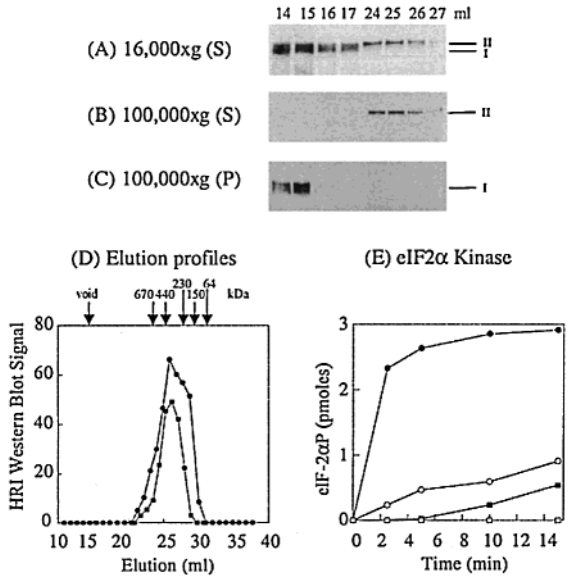

FIGURE 4: Molecular sizes of different species of HRI. The 16000*g* supernatant (panel A), 100000*g* supernatant (panel B), and 100000*g* pellet (panel C) from an overnight expression of HRI at 22.5 °C were separated by a Sephacryl S-400 column as described under Experimental Procedures. The positions of the elution of the molecular size standards and the void are marked in panel D. The elution profile of HRI was determined by SDS−PAGE followed by Western blot analysis using anti-HRI as described above. The peak fractions of void (14−17) and nonaggregated HRI (24−27) were shown side by side to demonstrate their different migration patterns on SDS−PAGE (panels A−C). To determine the molecular size of the species II HRI, 100000*g* supernatant was pretreated with TEV protease to remove the His tag of HRI prior to the gel filtration. A 100000*g* supernatant of mouse reticulocyte lysate served as control. The intensity of the Western blot signal of HRI in each fraction was quantitated by using NIH Image 6.1 software. The quantitation of elution profiles of reticulocyte HRI (●) and bacterial expressed HRI (■) was shown in panel D. In panel E 100000*g* supernatant (S-400 fraction 25, ●) and 100000*g* pellet (S-400 fraction 15, ■) were analyzed for specific eIF2α kinase activity of HRI in the absence (closed symbols) and presence (open symbols) of 2 μM heme. A time course from 0 to 15 min was performed. Specific activity is expressed as picomoles of eIF2α phosphorylated per nanogram of HRI.

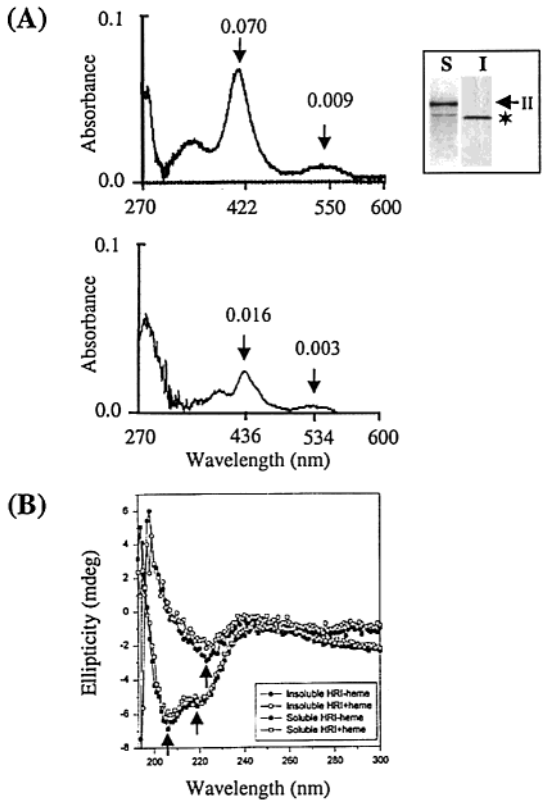

FIGURE 5: Hemoprotein spectra and CD spectra of purified soluble and insoluble HRI. Soluble (S) and insoluble (I) $(His)_6$-HRI were purified from the 16000*g* supernatant and pellet by Ni^{2+}−agarose column chromatography as described in Experimental Procedures. Purified proteins were separated by 10% PAGE and stained with Coomassie brilliant blue G250 (insert panel A). Full-length soluble and insoluble $(His)_6$-HRI were marked with an arrow and a star, respectively. (A) Hemoprotein spectra. His-tag-cleaved purified proteins (2.5 μM) incubated with 5 μM heme were scanned from 270 to 600 nm using 5 μM heme as a reference. The Soret band around 420 nm and the broad α and β bands around 550 nm are indicated by arrows. (B) CD spectra. Purified soluble (○) and insoluble (●) HRI (24 μM) were scanned from 180 to 300 nm. Heme-bound soluble and insoluble HRI (open symbols) were saturated with 100 μM heme, and the excess of heme was removed by dialysis.

affect the heme loading (not shown), we presume that the His tag further elongates the shape of HRI. Analysis of the eIF2α kinase activities using equal amounts of species I and species II HRI showed that species II dimeric HRI had a 200-fold higher specific eIF2α kinase activity that was regulated by heme (Figure 4E) with an apparent K_i of 0.22 μM (not shown), similar to reticulocyte HRI and recombinant HRI expressed in insect cells (*7*, *41*). These results indicate that multiple autophosphorylation is critical to maintaining HRI as a dimer and preventing aggregation.

Secondary Structure and Heme Binding of Purified Soluble and Insoluble HRI. To further characterize the structure and heme binding of soluble and insoluble HRI, both forms were purified to near homogeneity (Figure 5A, insert). Pure soluble HRI consisted mainly of species II. It migrated substantially slower than the insoluble HRI in SDS−PAGE, as seen by Coomassie blue staining (Figure 5A, insert). In agreement with the results shown above (Figures 1 and 2), only purified soluble HRI, and not the insoluble HRI, was highly phosphorylated on serine, threonine, and tyrosine residues, underwent autophosphorylation, and phosphorylated eIF2α (not shown). Purified soluble HRI was an active eIF2α kinase with a Michaelis−Menten constant (k_m) of 0.086 μM for the substrate eIF2α and a catalytic constant (k_{cat}) of 6.15×10^{-7} s^{-1}.

Without addition of exogenous heme, soluble HRI was only 5% saturated with heme during its expression in *E. coli* and thus exhibited only a small Soret band (not shown). In the presence of 5 μM heme, soluble HRI was saturated with heme and exhibited the absorption peaks of hemoproteins at 422 and 550 nm (Figure 5A, upper panel). The origin of the shoulder at 340 nm is not known and may reflect the presence of oxidized ferric heme (*45*). Measurement of heme content of heme-saturated HRI by pyridine hemochromogen (*46*) showed that it contained two molecules of heme per HRI monomer (not shown). This finding confirms our previous conclusion that there are two hemes bound per subunit of HRI (*41*) and that HRI has two separate heme-binding domains (*7*). Insoluble HRI (Figure 5A, lower panel) was less efficient in binding heme and exhibited only 20% of the heme-binding capacity of soluble HRI. In addition, the peak wavelength of the Soret band (436 nm) observed for insoluble HRI is different from that of the soluble HRI

(422 nm), suggesting a different conformation of the heme-binding domain of insoluble HRI.

To gain insight into the structural difference between soluble and insoluble HRI, CD spectroscopy was performed (Figure 5B). The CD spectrum of soluble HRI displayed the local minima at 206 and around 222 nm that are indicative of the presence of α-helical structure. In contrast, the CD spectrum of insoluble HRI exhibited a reduction in ordered secondary structure with a less pronounced 222 nm minimum and the absence of a 206 nm minimum. Collectively, these results indicate that insoluble HRI does not have the proper folding and conformation necessary for the solubility, kinase activity, and heme-binding activity of HRI. Neither the soluble nor the insoluble HRI exhibited a significant secondary structural change upon heme binding that can be detected by CD. However, heme binding to HRI could have an effect at the level of tertiary structure.

Multiple Phosphorylation of HRI in the Mouse Reticulocytes. To investigate the physiological importance of the differing extent of autophosphorylation of HRI, multiple phosphorylation of HRI naturally present in mouse reticulocytes was examined. Similar to HRI expressed in *E. coli*, HRI in mouse reticulocytes also exhibited two doublets with different electrophoretic mobilities in 10% SDS−PAGE. These two doublets of HRI in intact reticulocytes were better resolved into four species by 7.0% SDS−PAGE as shown in Figure 6A. In the hemin-treated reticulocytes, HRI was present mainly as species I with a very small amount of the lower band of species II (Figure 6A, left panel). It exhibited only little eIF2α kinase activity (Figure 6A, right panel). In the absence of hemin, HRI became activated. This activation resulted in the complete upshift of HRI to the slowest migrating species. This result indicates that in intact reticulocytes species I is in an inactive conformation as shown above for recombinant HRI species I (Figures 2 and 4). The activation of HRI in intact reticulocytes was accompanied by the increased eIF2αP in vivo (Figure 6A, right panel, lanes 1 and 3) while total eIF2α remained unchanged. Since there was no increase in the eIF2αP in $HRI^{-/-}$ reticulocytes (Figure 6A, right panel, lanes 2 and 4), this increase in eIF2αP in heme deficiency is due entirely to the activation of HRI.

The small increase in eIF2αP observed in hemin-treated Wt reticulocytes as compared to that of the $HRI^{-/-}$ reticulocytes (Figure 6A, right panel, lanes 3 and 4) was likely to originate from the small amount of species II present. To test this hypothesis, we separated the different species of HRI by HiTrapQ ion-exchange column chromatography according to their difference in negative charges. As shown in the left panel of Figure 6B, the majority of reticulocyte HRI species I was eluted with 0.3 M NaCl (lane 4) while species II was eluted with 0.35 M NaCl (lane 5). Recombinant species I and II HRI also eluted at the same NaCl concentrations as the corresponding reticulocyte HRI species (not shown). Reticulocyte HRI species II was found to possess 5-fold higher eIF2α kinase activity than species I (Figure 6B, right panel). It has a specific eIF2α kinase activity similar to that of species II recombinant HRI expressed in *E. coli*. Since species I HRI from reticulocytes is a dimer and is not aggregated (Figure 4D; *6*, *43*, *44*), it has a 40-fold higher specific eIF2α kinase activity than species I of HRI expressed in *E. coli*.

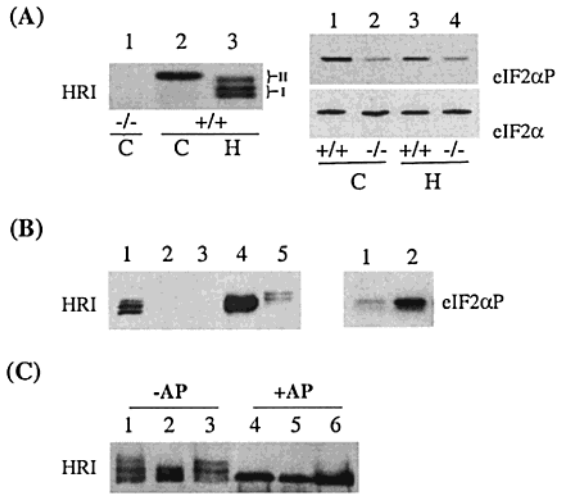

FIGURE 6: Multiple phosphorylation of HRI in mouse reticulocytes. (A) Activation of HRI in heme-deficient reticulocytes. Reticulocytes from $HRI^{+/+}$ and $HRI^{-/-}$ mice were incubated with 40 μM hemin (H) for 90 min. C denotes untreated control reticulocytes. Activation of HRI in the reticulocytes (1×10^6 cells) was analyzed using 7.0% SDS−PAGE followed by Western blot analysis. In parallel, the eIF2α phosphorylation in intact reticulocytes was also analyzed by anti-eIF2α phosphorylated antibody (upper right panel). The total amount of eIF2α is shown in the lower right panel. (B) HiTrapQ ion-exchange chromatography of HRI in mouse reticulocyte lysates. Mouse reticulocyte lysates (lane 1) were separated by HiTrapQ chromatography as described under Experimental Procedures. The flow-through of the HiTrapQ column (lane 2), the 0.2 M NaCl wash (lane 3), and the peak fractions of elution with 0.3 M NaCl (lane 4) and with 0.35 M NaCl (lane 5) were separated by 7.5% SDS−PAGE. HRI was detected by Western blot analysis using anti-HRI antibody. Equal amounts of the HRI eluted with 0.3 M (right panel, lane 1) and 0.35 M NaCl (right panel, lane 2) were assayed for eIF2α kinase activity. (C) Alkaline phosphatase treatment. Mouse reticulocyte lysates (lanes 1 and 4) and the peak fractions of elution with 0.3 M (lanes 2 and 5) and with 0.35 M NaCl (lanes 3 and 6) were incubated for 15 min at 30 °C with or without alkaline phosphatase (AP) as indicated. HRI was analyzed by Western blot analysis using anti-HRI antibody.

Since reticulocyte species II has a slower electrophoretic mobility than species I and elutes with higher salt concentration from the HiTrapQ column, we sought to demonstrate that reticulocyte species II HRI are more extensively phosphorylated than species I, similar to HRI species expressed in bacteria using alkaline phosphatase treatment. As shown in Figure 6C, dephosphorylation by alkaline phosphatase converted the slower migrating species II of reticulocyte HRI to the fastest migrating species. These results demonstrate the presence of multiply phosphorylated species of HRI in intact reticulocytes and the activation of HRI by phosphorylation in heme-deficient intact reticulocytes.

DISCUSSION

In reticulocyte lysates, HRI is thought to be present in an inactive proinhibitor form (ProHRI) which is converted in heme deficiency to a heme-reversible active form (reviewed in ref *43*). The structural difference between these two forms of HRI has yet to be elucidated. In this study, we demonstrate that multiple autophosphorylation of HRI is responsible for the conversion of inactive ProHRI to heme-reversible HRI. We also show that recombinant HRI expressed in *E. coli* exhibits the same degree of multiple autophosphorylation as HRI naturally present in reticulocytes. Similarly, it has been

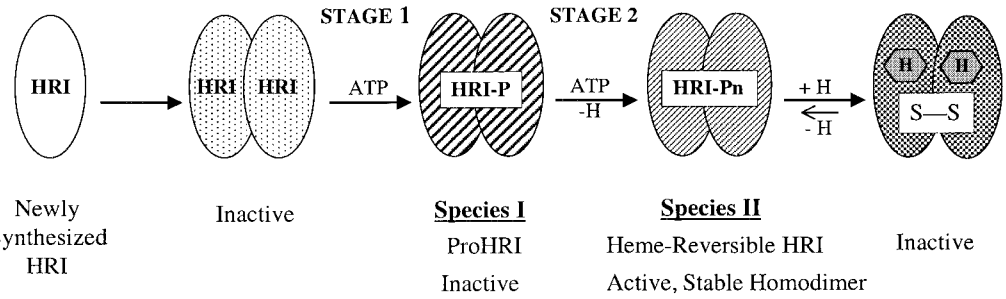

FIGURE 7: Model of the formation of active stable HRI by two-staged multiple autophosphorylation.

shown that the catalytic subunit of PKA expressed in *E. coli* exhibits all autophosphorylation present in the enzyme purified from mammalian tissues (*47*, *48*).

A model based upon our findings on the formation of active HRI is presented in Figure 7. We propose that newly synthesized HRI is rapidly dimerized and undergoes intermolecular multiple autophosphorylation in two stages. The first stage phosphorylation of HRI results in the formation of inactive species I. Additional phosphorylation at the second stage in heme deficiency results in the formation of active species II HRI. This autophosphorylation of HRI occurs mainly on Ser and Thr residues and to a lesser extent on Tyr residues (Figures 1−3) and reduces the electrophoretic mobility of HRI as shown in Figures 1 and 6.

The difference in degree of phosphorylation between species I and II permitted their separation by ion-exchange chromatography and the subsequent biochemical characterization of these two forms of HRI. Since the less phosphorylated species I is present in the heme-supplemented intact reticulocytes only (Figure 6A), recombinant HRI species I observed in *E. coli* resembles the ProHRI. We found that species I of recombinant HRI and species I of reticulocyte HRI (Figure 6B) elute at lower ionic strength than species II. In addition, species I HRI from reticulocytes and that from *E. coli* expression both have a very weak eIF2α kinase activity. The more extensively phosphorylated species II HRI is equivalent to heme-reversible HRI in that species II HRI is an active eIF2α kinase and its kinase activity is regulated by heme both in vitro (Figure 4) and in vivo (Figure 6A). The apparent K_i of 0.22 μM for the hemin inhibition of species II HRI expressed in *E. coli* is the same as that of HRI in reticulocytes and HRI expressed in insect cells (*41*). In addition, upon addition of exogenous heme, purified species II HRI expressed in *E. coli* displayed the typical visible spectrum of a hemoprotein (Figure 5A) as the HRI expressed in insect cells (*41*).

It was reported earlier that HRI in reticulocytes is associated with the chaperones Hsp90 and Hsc70 (*34*, *49*, *50*). These chaperones are required to keep HRI from denaturation and aggregation (*34*). We found here that species I HRI expressed in *E. coli* formed aggregates despite remaining soluble at 16000*g*. This observation is consistent with the limiting amount of chaperones in *E. coli* under high-level protein expression conditions. It may also account for the reason ProHRI could not be purified from reticulocytes beyond certain stages (*51*). We speculate that the loss of ProHRI during purification is due to the removal of the chaperones from ProHRI and subsequent aggregation similarly to that observed to occur with species I HRI from *E. coli* expression. The tendency of species I HRI to aggregate could also explain why it could not be converted completely to species II in vitro either in *E. coli* extracts or in the purified protein (not shown).

HRI that does not undergo autophosphorylation migrates fastest in SDS−PAGE, is aggregated, and is insoluble as demonstrated by the K196R mutant HRI and the insoluble pellet of Wt HRI (Figure 2). In contrast, species II HRI is much more stable and remains soluble at 100000*g* as a homodimer (Figure 4). Moreover, the stabilization of HRI by autophosphorylation is so effective that recombinant HRI can be expressed in *E. coli* at concentrations 1000-fold that present in reticulocytes. This observation is consistent with previous biochemical studies which demonstrate that heme-reversible HRI is a stable homodimer (reviewed in ref *1*). Thus, multiple autophosphorylation of HRI is required not only for the activation of its eIF2α kinase activity but also for the stabilization of HRI as a homodimer. Our data provide in vivo evidence for a novel function of autophosphorylation in maintaining the stabilility and solubility of HRI. In this respect, HRI is very similar to the C-subunit of PKA. Autophosphorylation of the newly synthesized C-subunit at Ser338 and Ser10 is necessary for kinase stability and solubility, respectively, of PKA (*52*, *53*). Similarly, also *Xenopus* c-Mos serine/threonine kinase is only partially phosphorylated and is unstable in the early step of meiotic maturation but is fully phosphorylated and highly stable in the late step. Phosphorylations on Ser3 and Ser16 are important for this stabilization (*54*, *55*). Our finding together with these other examples suggests that multiple autophosphorylation might be a general mechanism for stabilizing kinases.

Here, we also show that HRI undergoes autotyrosine phosphorylation. The biological significance of this finding has yet to be examined. Interestingly, a number of serine/threonine kinases such as members of the LAMMER kinase family, glycogen synthase 3 and Clk2, also undergo tyrosine phosphorylation when expressed in *E. coli* (*56*, *57*) and in eukaryotes. These kinases are now considered to belong to the steadily growing class of dual specificity kinases.

The availabilities of purified species I and species II HRI demonstrated in this study permit us to identify the phosphorylation sites that occur in each of the two-staged activation of HRI. We are currently identifying the autophosphorylation sites of HRI and plan to introduce point mutations to analyze their functions individually.

In summary, our study provides in vivo evidence that autophosphorylation of HRI at multiple sites soon after its de novo synthesis regulates HRI in a two-stage mechanism. The first stage of phosphorylation stabilizes species I HRI against aggregation. We provide compelling evidence that

this species I HRI is the ProHRI that was postulated in 1972 (*58*). The second-stage multiple phosphorylation is critical to stabilizing HRI as a homodimer and is required for the attainment of eIF2α kinase activity that is regulated by heme.

ACKNOWLEDGMENT

We thank Dr. Ron Wek, Department of Biochemistry and Molecular Biology, Indiana University School of Medicine, for providing the plasmid of yeast eIF2α, Dr. Shuguang Zhang, Department of Biology, Massachusetts Institute of Technology, for making the CD instrument available, and Dr. Jane Yang, Department of Pathology, Massachusetts General Hospital, Harvard Medical School, for critical reading of the manuscript.

REFERENCES

1. Chen, J.-J. (2000) in *Translational Control of Gene Expression* (Sonnenberg, N., Hershey, J. W. B., and Mathews, M. B., Eds.) pp 529−546, Cold Spring Harbor Laboratory Press, Cold Spring Harbor, NY.
2. Krishnamoorthy, T., Pavitt, G. D., Zhang, F., Dever, T. E., and Hinnebusch, A. G. (2001) *Mol. Cell. Biol. 21*, 5018−5030.
3. Hershey, J. W. B., and Merrick, W. C. (2000) in *Translational Control of Gene Expression* (Sonnenberg, N., Hershey, J. W. B., and Mathews, M. B., Eds.) pp 33−88, Cold Spring Harbor Laboratory Press, Cold Spring Harbor, NY.
4. Crosby, J. S., Lee, K., London, I. M., and Chen, J.-J. (1994) *Mol. Cell. Biol. 14*, 3906−3914.
5. Chen, J.-J., Yang, J. M., Petryshyn, R., Kosower, N., and London, I. M. (1989) *J. Biol. Chem. 264*, 9559−9564.
6. Yang, J. M., London, I. M., and Chen, J.-J. (1992) *J. Biol. Chem. 267*, 20519−20524.
7. Rafie-Kolpin, M., Chefalo, P. J., Hussain, Z., Hahn, J., Uma, S., Matts, R. L., and Chen, J.-J. (2000) *J. Biol. Chem. 275*, 5171−5178.
8. Chen, J.-J. (1993) in *Translational Control of Gene Expression 2* (Ilan, J., Ed.) pp 349−372, Plenum Press, New York.
9. Chen, J.-J., and London, I. M. (1995) *Trends Biochem. Sci. 20*, 105−108.
10. Clemens, M. J. (1996) in *Translational Control of Gene Expression* (Sonnenberg, N., Hershey, J. W. B., and Mathews, M. B., Eds.) pp 139−172, Cold Spring Harbor Laboratory Press, Cold Spring Harbor, NY.
11. Williams, B. R. G. (1999) *Oncogene 18*, 6112−6120.
12. Shi, Y., Vattem, K. M., Sood, R., An, J., Liang, J., Stramm, L., and Wek, R. C. (1998) *Mol. Cell. Biol. 18*, 7499−7509.
13. Harding, H. P., Zhang, Y., and Ron, D. (1999) *Nature 397*, 271−274.
14. Sood, R., Porter, A. C., Ma, K., Quilliam, L. A., and Wek, R. C. (2000) *Biochem. J. 346*, 281−293.
15. Hinnebusch, A. G. (1996) in *Translational Control of Gene Expression* (Sonnenberg, N., Hershey, J. W. B., and Mathews, M. B., Eds.) pp 199−244, Cold Spring Harbor Laboratory Press, Cold Spring Harbor, NY.
16. Santoyo, J., Alcalde, J., Mendez, R., Pulido, D., and De Haro, C. (1997) *J. Biol. Chem. 272*, 12544−12550.
17. Sattleger, E., Hinnebush, A. G., and Barthelemes, I. B. (1998) *J. Biol. Chem. 273*, 20404−20416.
18. Berlanga, J. J., Santoyo, J., and De Haro, C. (1999) *Eur. J. Biochem. 265*, 754−762.
19. Berlanga, J. J., Herrero, S., and de Haro, C. (1998) *J. Biol. Chem. 273*, 32340−32346.
20. Chen, J.-J., Throop, M. S., Gehrke, L., Kuo, I., Pal, J. K., Brodsky, M., and London, I. M. (1991) *Proc. Natl. Acad. Sci. U.S.A. 88*, 7729−7733.
21. Chong, K. L., Schappert, K., Meurs, E., Feng, F., Donahue, T. F., Friesen, J. D., Hovanessian, A. G., and Williams, B. R. G. (1992) *EMBO J. 11*, 1553−1562.
22. Meurs, E., Chong, K., Galabru, J., Thomas, N. S. B., Kerr, I. M., Williams, B. R. G., and Hovanessian, A. G. (1990) *Cell 62*, 379−390.
23. Ramirez, M., Wek, R. C., and Hinnebusch, A. G. (1991) *Mol. Cell. Biol. 11*, 3027−3036.
24. Colthurst, D. R., Campbell, D. G., and Proud, C. G. (1987) *Eur. J. Biochem. 166*, 357−363.
25. Dever, T. E., Chen, J.-J., Barber, G. N., Cigan, A. M., Feng, L., Donahue, T. F., London, I. M., Katze, M. G., and Hinnebusch, A. G. (1993) *Proc. Natl. Acad. Sci. U.S.A. 90*, 4616−4620.
26. Kaufman, R. J. (2000) in *Translational Control of Gene Expression* (Sonnenberg, N., Hershey, J. W. B., and Mathews, M. B., Eds.) pp 503−528, Cold Spring Harbor Laboratory Press, Cold Spring Harbor, NY.
27. Clemens, M. J., and Elia, A. (1997) *J. Interferon Cytokine Res. 17*, 503−524.
28. Hinnebusch, A. G. (2000) in *Translational Control of Gene Expression* (Sonnenberg, N., Hershey, J. W. B., and Mathews, M. B., Eds.) pp 185−244, Cold Spring Harbor Laboratory Press, Cold Spring Harbor, NY.
29. Thomis, D. C., and Samuel, C. E. (1993) *J. Virol. 67*, 7695−7700.
30. Thomis, D. C., and Samuel, C. E. (1995) *J. Virol. 69*, 5195−5208.
31. Taylor, D. H., Lee, S. B., Romano, P. R., Marshak, D. R., Hinnebush, A. G., Esteban, M., and Mathews, M. B. (1996) *Mol. Cell. Biol. 16*, 6295−6302.
32. Romano, P. R., Garcia-Barrio, M. T., Zhang, X., Wang, Q., Taylor, D. R., Zhang, F., Herring, C., Mathews, M. B., Qin, J., and Hinnebush, A. G. (1998) *Mol. Cell. Biol. 18*, 2282−2297.
33. Zhang, F., Romano, P. R., Nagamura-Inoue, T., Tian, B., Dever, T. E., Mathews, M. B., Ozato, K., and Hinnebusch, A. G. (2001) *J. Biol. Chem. 276*, 24946−24958.
34. Uma, S., Hartson, S. D., Chen, J.-J., and Matts, R. L. (1997) *J. Biol. Chem. 272*, 11648−11656.
35. Chefalo, P. J., Yang, J. M., Ramaiah, K. V. A., Gehrke, L., and Chen, J.-J. (1994) *J. Biol. Chem. 269*, 25788−25794.
36. Duclos, B., Marcandier, S., and Cozzone, A. J. (1991) *Methods Enzymol. 201* (Part B), 10−20.
37. Zhu, S., Sobolev, A. Y., and Wek, R. C. (1996) *J. Biol. Chem. 271*, 24989−24994.
38. DeGracia, D. J., Sullivan, J. M., Neumar, R. W., Alousi, S. S., Hikade, K. R., Pittman, J. E., White, B. C., Rafols, J. A., and Krause, G. S. (1998) *J. Cereb. Blood Flow Metab. 18*, 876−881.
39. Scorsone, K. A., Panniers, R., Rowlands, A. G., and Henshaw, E. C. (1987) *J. Biol. Chem. 262*, 14538−14543.
40. Kennelly, P. J., and Potts, M. (1996) *J. Bacteriol. 178*, 4759−4764.
41. Chefalo, P., Oh, J., Rafie-Kolpin, M., and Chen, J.-J. (1998) *Eur. J. Biochem. 258*, 820−830.
42. Chen, J.-J., Pal, J. K., Petryshyn, R., Kuo, I., Yang, J. M., Throop, M. S., Gehrke, L., and London, I. M. (1991) *Proc. Natl. Acad. Sci. U.S.A. 88*, 315−319.
43. Hunt, T. (1979) in *Miami Winter Symposium: From Gene to Protein* (Russel, T. R., Brew, K., Schultz, J., and Haber, H., Eds.) pp 16, 321−345, Academic Press, New York.
44. Gross, M., Olin, A., Hessefort, S., and Bender, S. (1994) *J. Biol. Chem. 269*, 22738−22748.
45. Aono, S., Ohkubo, K., Matsuo, T., and Nakajima, H. (1998) *J. Biol. Chem. 273*, 25757−25764.
46. Rieske, J. S. (1967) *Methods Enzymol. 10*, 488−493.
47. Shoji, S., Titani, K., Demaille, J. G., and Fischer, E. H. (1979) *J. Biol. Chem. 254*, 6211−6214.
48. Toner-Webb, J., van Patten, S. M., Walsh, D. A., and Taylor, S. S. (1992) *J. Biol. Chem. 267*, 25174−25180.
49. Matts, R. L., Xu, Z., Pal, J. K., and Chen, J.-J. (1992) *J. Biol. Chem. 267*, 18160−18167.
50. Uma, S., Thulasiraman, V., and Matts, R. L. (1999) *Mol. Cell. Biol. 19*, 5861−5871.

51. Hunt, T., Vanderhoff, G. A., and London, I. M. (1972) *J. Mol. Biol. 66*, 471−481.
52. Steinberg, R. A., Cauthron, R. D., Symcox, M. M., and Shuntoh, H. (1993) *Mol. Cell. Biol. 13*, 2332−2341.
53. Yonemoto, W., McGlone, M. L., Grant, B., and Taylor, S. S. (1997) *Protein Eng. 10*, 915−925.
54. Nishizawa, M., Okazaki, K., Furuno, N., Watanabe, N., and Sagata, N. (1992) *EMBO J. 11*, 2433−2446.
55. Pham, C. D., Vuyyuru, V. B., Yang, Y., Bai, W., and Singh, B. (1999) *Oncogene 18*, 4287−4294.
56. Howell, B. W., Afar, D. E., Lew, J., Douville, E. M., Icely, P. L., Gray, D. A., and Bell, J. C. (1991) *Mol. Cell. Biol. 11*, 568−572.
57. Hughes, K., Nikolokaki, E., Plyte, S. E., Totty, N. F., and Woodgett, J. R. (1993) *EMBO J. 12*, 803−808.
58. Gross, M., and Rabinovitz, M. (1972) *Proc. Natl. Acad. Sci. U.S.A. 69*, 1565−1568.

BI010983S